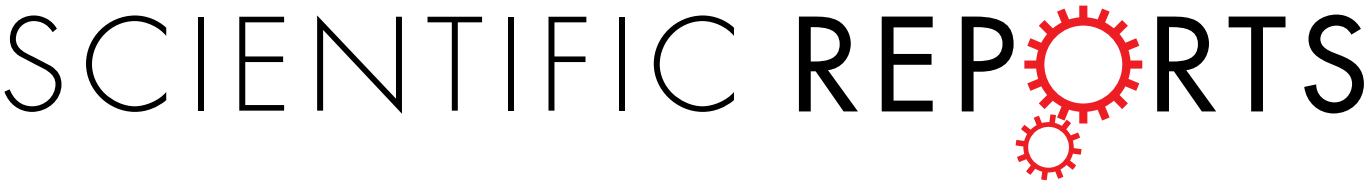

OPEN

Anion-controlled dimer distance induced unique solid-state fluorescence of cyano substituted styrene pyridinium

Received: 14 July 2016
Accepted: 01 November 2016
Published: 21 November 2016

Gaobin Zhang[1], Xuanjun Zhang[2], Lin Kong[1], Shichao Wang[2], Yupeng Tian[1], Xutang Tao[3] & Jiaxiang Yang[1,3]

Molecular packing arrangements play a key role in dominating the photophysical properties of luminophores in aggregated state but fine control of the molecular packing is a great challenge. This article describes a unique cyano substituted styrene pyridinium with interesting solid-state fluorescence that can be finely tuned by simple change of counteranions. The dilute solutions of the organic salts (PyCl, $PyNO_3$, PyOTs and $PyPh_4B$) exhibit very weak fluorescence. The crystals of the organic salts (PyCl, $PyNO_3$, and PyOTs) show much enhanced fluorescence compared with their dilute solutions. It is interesting that the emissions changed from bluish-green to deep-blue and fluorescence quantum yields increase from 2.5% to 13.1% with the increasing of steric hindrance of the anions from chloridion, nitrate, to p-toluenesulfonate. Crystal and DFT studies reveal that the enhanced fluorescence is ascribed to the formation of dimers and bigger anions induce larger molecular separation in dimers. Tetraphenylboron anion with very large steric hindrance impedes the formation of dimers and thus results in non-fluorescent salt ($PyPh_4B$). Meanwhile, this unique dimeric packing endows the crystal of $PyNO_3$ with anisotropic fluorescence.

Conjugated organic luminophors have wide applications in organic light-emitting diode (OLEDs)[1–5], smart materials[6–10] and sensors[11–15]. Understanding the structure-property relationship is very important to guide the design of correct molecules for their providential applications[16–23]. Artful molecular design through varying molecular backbone substituent groups and effective π-conjugation lengths or impacting the intra/intermolecular interactions to achieve high emission in the solid state is the most common method[24–28]. In contrast the notorious aggregation-caused quenching (ACQ), branchy and twisted aggregation-induced emission (AIE) and aggregation-induced emission enhancement (AIEE) fluorogens are developed to tune the intermolecular stacking for efficient emissions in the solid state[29–32]. Alternative ways to regulate multifunctional materials are allomorphism and mischcrystal[33–35]. This strategy do not involves tedious organic synthesis. However, the requirements for the molecular structures are stringent and the distinct properties commonly disappear when the crystals are damaged.

Organic salts have advantages for the design of solid-state emitters because the photophysical properties could be tuned by both their cation and anion constituents[36–43]. The cationic fluorogens are usually designed with complex and flexible structures to against the strong dipole-dipole interactions, which open the non-radiation decay channels and thus quench the solid-state luminescence. The changes of the anions would also greatly influence the emission in aggregation of organic salts because the strength of electrostatic attraction between cationic and anionic species and steric hindrance may deeply affect the molecular packing in aggregation[44–51]. Bhattacharya, *et al.* reported a phenylenedivinylene bis-N-octyl pyridinium salt[52]. The salt effect profoundly influenced the order of aggregation of the gelator molecules to form a novel chromophore assembly leading to an aggregation-induced switch of the emission colors. Tang's group found that effect of the counterion could change the emission behavior

[1]College of Chemistry & Chemical Engineering, Key Laboratory of Functional Inorganic Materials of Anhui Province, Anhui University, Hefei 230601, P. R. China. [2]Faculty of Health Sciences, University of Macau, Taipa, Macau SAR, P. R. China. [3]State Key Laboratory of Crystal Materials, Shandong University, Jinan 502100, P. R. China. Correspondence and requests for materials should be addressed to X.Z. (email: xuanjunzhang@umac.mo) or J.Y. (email: jxyang@ahu.edu.cn)

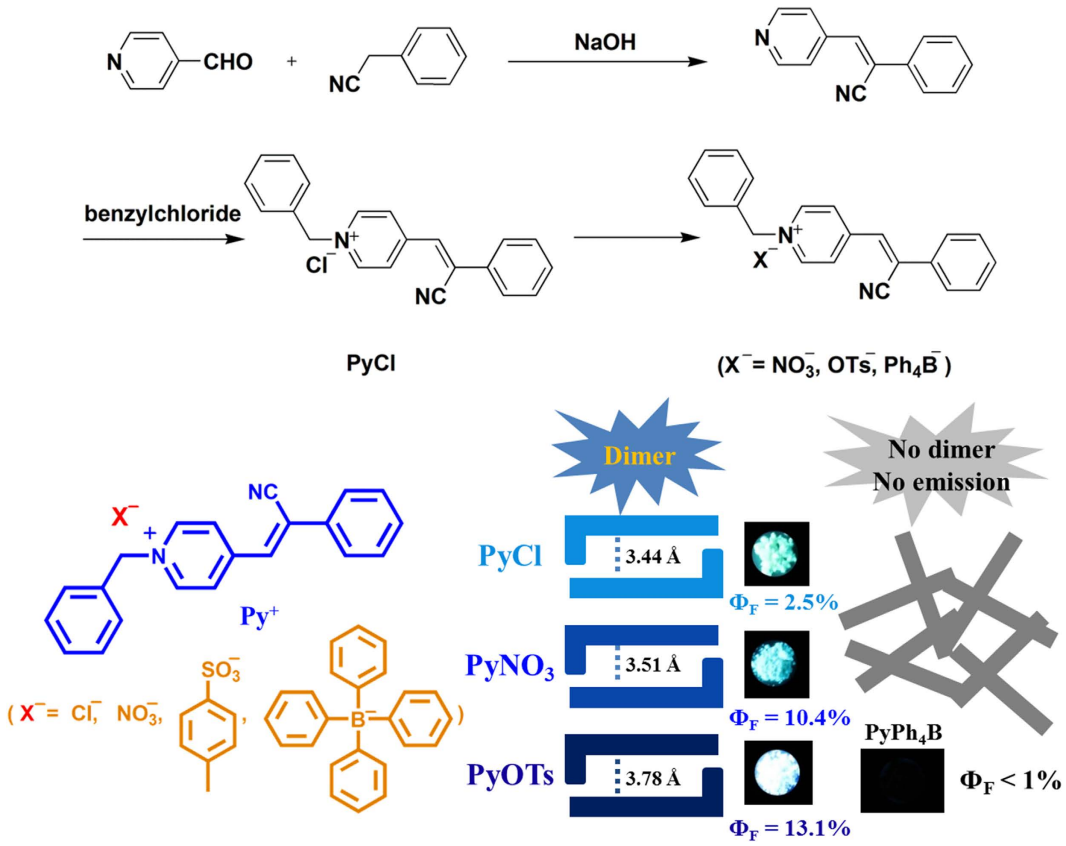

Figure 1. The synthetic routes of compounds and schematic illustration of packing arrangements.

of (TPE)-functionalized benzothiazolium salts from ACQ to AIE[53]. While a number of literatures focus on the effect of the counterion on the photophysical characteristics of organic salts, the definite and visual evidences of the structure-property relationship are seldom reported as far as we know.

In this work, a series of cyano substituted styrene pyridinium salts (Fig. 1) were prepared, which exhibited unique anion-controlled solid-state fluorescence. The compound **PyCl** was synthesized in high yield using pyridylaldehyde and phenylacetonitrile by Knoevenagel reaction followed by reaction with benzylchloride. **$PyNO_3$**, **PyOTs**, and **$PyPh_4B$** were obtained by exchange of the anions in methanol using silver nitrate, silver p-toluenesulfonate and tetraphenylborate, respectively. It is interesting that these four organic salts exhibit remarkable differences in solid-state fluorescence.

Results and Discussion

To investigate the effect of counterion, the photophysical properties of **PyCl**, **$PyNO_3$**, **PyOTs** and **$PyPh_4B$** in various dilute organic solvents with different polarities are firstly studied. As depicted in Fig. 2, the absorption and fluorescence spectra of the all compounds in dilute solutions show similar profiles. The main peaks of their absorption spectra locate at about 345 nm, which have very little changes in different organic solvents (Figure S1). Meanwhile, evidence solvatochromic effects were observed (Figure S2). With the increasing of the polarity of solvents, the emission peaks showed red-shifted from about 420 nm to about 445 nm, which indicated a strong intramolecular charge transfer (ICT). The Lippert–Mataga relation was used to better understand the solvent-polarity effect. Interestingly, the plot of the orientation polarizability (Δf) versus the Stokes' shift of the compounds shows two sets of linearity indicative of two different excited states (Fig. 2b and Figures S3–5). The larger slope in the strong polarity solvents shows a typical character of CT state[54]. All above, the similar Lippert-Mataga relation, absorption and fluorescence of **PyCl**, **$PyNO_3$**, **PyOTs** and **$PyPh_4B$** in various dilute organic solvents in which molecules are monomers indicate that the anions have no effect on the photophysical properties of the cationic fluorogen and the interactions between cations and anions could not change the decay channel of cationic fluorogen monomers.

The strengthened interactions between anions and cations in the solid state have deep effect on the intra/intermolecular packing arrangements, which could be reflected on the photophysical properties. The pyridinium salt is easily dissolved in the polar solvents such as MeOH, EtOH, acetonitrile and DMF, but insoluble in toluene, benzene and THF. Solvent/non-solvent experiments were carried out to investigate the aggregation behaviors by controlling the acetonitrile/toluene ratios. The absorption (Figure S6) and fluorescence (Figure S7) spectra of **PyCl**, **$PyNO_3$**, **PyOTs** and **$PyPh_4B$** were found to be dependent on the toluene fraction. All of the compounds in acetonitrile is weakly emissive because of the twisted intermolecular charge transfer (TICT). When the non-solvent toluene is added, the fluorescence spectra of **PyCl**, **$PyNO_3$** and **PyOTs** present almost the same

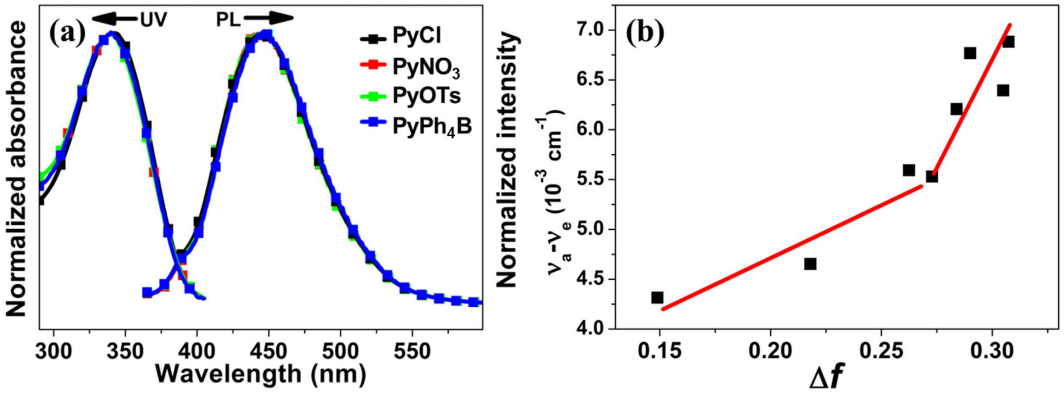

Figure 2. **(a)** Absorptions and fluorescence spectra of the four compounds in acetonitrile (10 μM). **(b)** Linear correlation of the Stokes' shift with the solvents orientation polarization for **PyCl**.

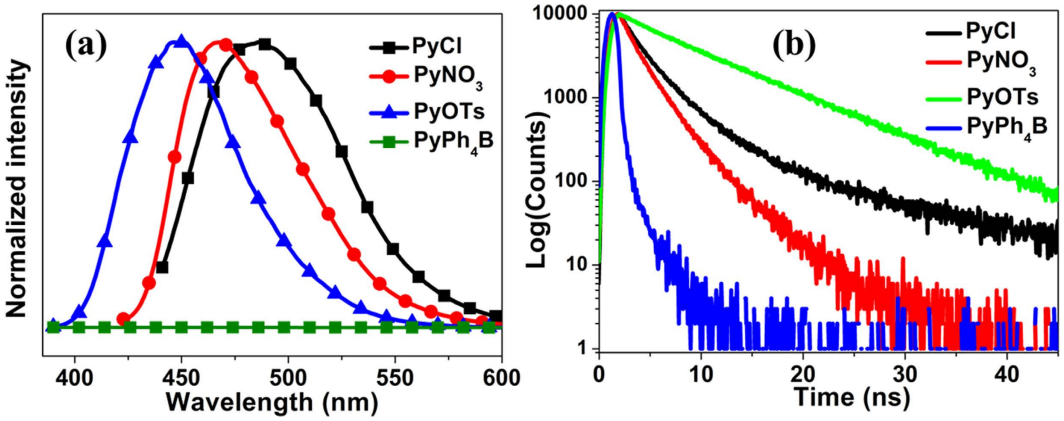

Figure 3. **(a)** Fluorescence spectra and **(b)** lifetimes of the compounds in the solid state.

Compounds	λ_{em}[a] (nm)	Φ_F[b] (%)	Φ_F[c] (%)	τ[e] (ns)	τ[f] (ns)
PyCl	486	2.5	0.2	0.14	2.71
$PyNO_3$	467	10.4	0.3	0.26	1.85
PyOTs	448	13.1	0.1	0.16	7.81
$PyPh_4B$	—	<1	—	0.11	0.1

Table 1. Photophysical properties of the compounds. [a]Emission wavelength in the solid state. [b]Absolute fluorescence quantum yields of solids determined by a calibrated integrating sphere. [c]Absolute fluorescence quantum yields in acetonitrile of compounds determined by a calibrated integrating sphere. [d]Fluorescence lifetimes in acetonitrile. [e]Fluorescence lifetimes of the solid samples.

tendency. With the increasing of the toluene fractions (f_T), the maximal emission gradually enhanced. It is noted that the maximal intensity of **PyCl**, **$PyNO_3$** and **PyOTs** is increased with the increasing of the steric of the anions. These results reveal that **PyCl**, **$PyNO_3$** and **PyOTs** are AIEE active. Very interestingly, **$PyPh_4B$** with the largest anion shows weak emission both in dilute solution and aggregate without AIEE effect. The fluorescence intensity was gradually decreased with the increasing of f_T in acetonitrile/toluene mixture. The results demonstrate that the aggregation of **$PyPh_4B$** is difference from those of **PyCl**, **$PyNO_3$** and **PyOTs** and the molecular packing arrangements are anion-dependent.

The solid-state fluorescence was also investigated using microcrystals. As shown in Fig. 3, the emission wavelengths of **PyCl**, **$PyNO_3$** and **PyOTs** are at 486, 467 and 448 nm, respectively, which indicate that the fluorescence are blue-shifted with the increasing of steric of anions. Fluorescence quantum yields (Φ_F) of **PyCl**, **$PyNO_3$**, **PyOTs** and **$PyPh_4B$** in the solid state were determined by a calibrated integrating sphere. The Φ_F values of these compounds were quite different (Table 1). **PyOTs** with the second larger anions exhibits the highest Φ_F value of 13.1%. However, **$PyPh_4B$** with the largest anion of tetraphenyl borate is nearly non-emissive in the solid state ($\Phi_F < 1\%$). The Φ_F value of **$PyNO_3$** is 10.4%, which is higher than that of **PyCl** (2.5%).

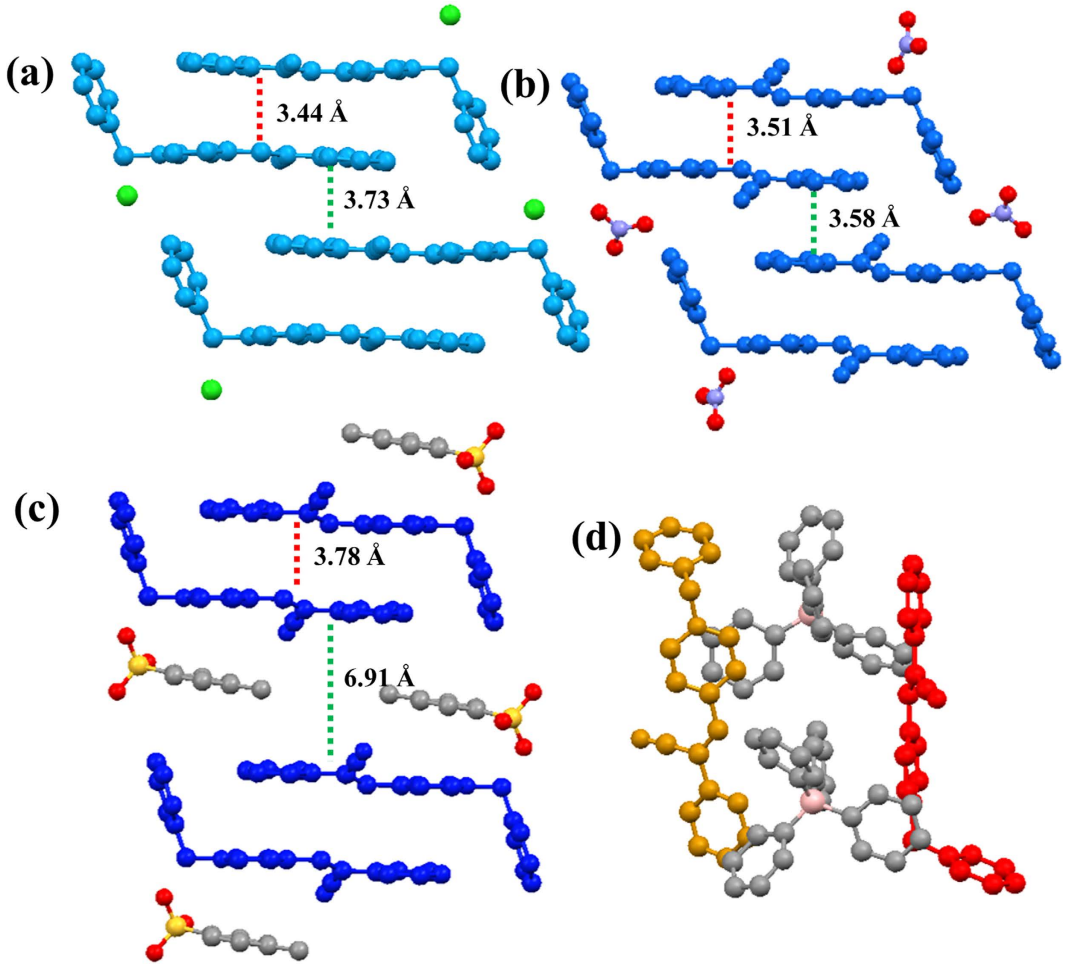

Figure 4. The molecular packing arrangements in crystals **PyCl (a)**, **$PyNO_3$ (b)**, **PyOTs (c)** and **$PyPh_4B$ (d)**.

Crystallographic studies are important to understand the roles of anions on the packing arrangement and the fluorescence mechanism. Fortunately, single crystals suitable for X-ray diffraction were obtained for all of the four salts. The detailed crystal and structure refinement data are given in Table S1. The packing arrangements of **PyCl**, **$PyNO_3$**, **PyOTs** are "bricks" with the anions inserted in the space between cationic fluorogens (Figures S8–10). However, the molecular packing of **$PyPh_4B$** is different from the others (Figure S11). The molecular packing is stabilized by multiple interactions between the cations and anions. The steric effects of anions significantly affect the molecular planarity and packing of the cations. The monatomic chloridion in **PyCl** formed three H-bond on the same plane leading to better planarity of the cation, in which the pyridyl, vinyl and phenyl are almost co-planar. However, the nitrate anion is in a polyhedron conformation. Different oxygen atoms of nitrate anion form three H-bonds with the H atoms located at the pyridyl, vinyl, and phenyl, respectively, which results in a twisted structure. In the crystal of **PyOTs** with larger anion p-toluenesulfonate, the cations are also non-planar (Figures S12–13).

The D-π-A type molecules have the tendency to form H-aggregate by the coulombic force[55–58]. The **PyCl**, **$PyNO_3$** and **PyOTs** formed H-aggregate dimers by the face-to-face stacking of the electron-deficient pyridinium cation and the relative electron-rich phenyl. Moreover, the degree of π-π stacking of **PyCl**, **$PyNO_3$** and **PyOTs** dimers are controlled by the multiple interactions between cations and anions through conducting the distance of the paired molecules (Fig. 4). In the crystal of **PyCl**, as a result of the planarity structure of cation and small size of anion, the distance between two monomers in a dimeric pair is short (3.44 Å), which indicates the strong π-π stacking between the paired molecules. Affected by the steric hindrance of nitrate anions, the intradimeric distance of **$PyNO_3$** was 3.51 Å, which was slightly longer than that in **PyCl**. Distance between the paired molecules of in **PyOTs** was the longest (3.78 Å), which indicates a weak π-π stacking between the paired monomers. Besides, the C-H$_{\cdots}$π and H-bond interactions between the anions and cations increased the overlap of the paired molecules. Thus, the steric hindrance of anions tune the distance between two dimeric molecules that result in the different degree of intradimeric interactions.

On the other hand, the distance between neighboring dimers was dominated by both the ionic interaction and steric hindrance. The dimer to dimer distance in **$PyNO_3$** crystal was 3.58 Å, which was shorter than that of 3.73 Å in **PyCl**. We found that dimers in **$PyNO_3$** were drawn up by several H-bonds between nitrate anion and two neighboring dimers. While, there is no direct interaction between chloridion and neighboring dimers in

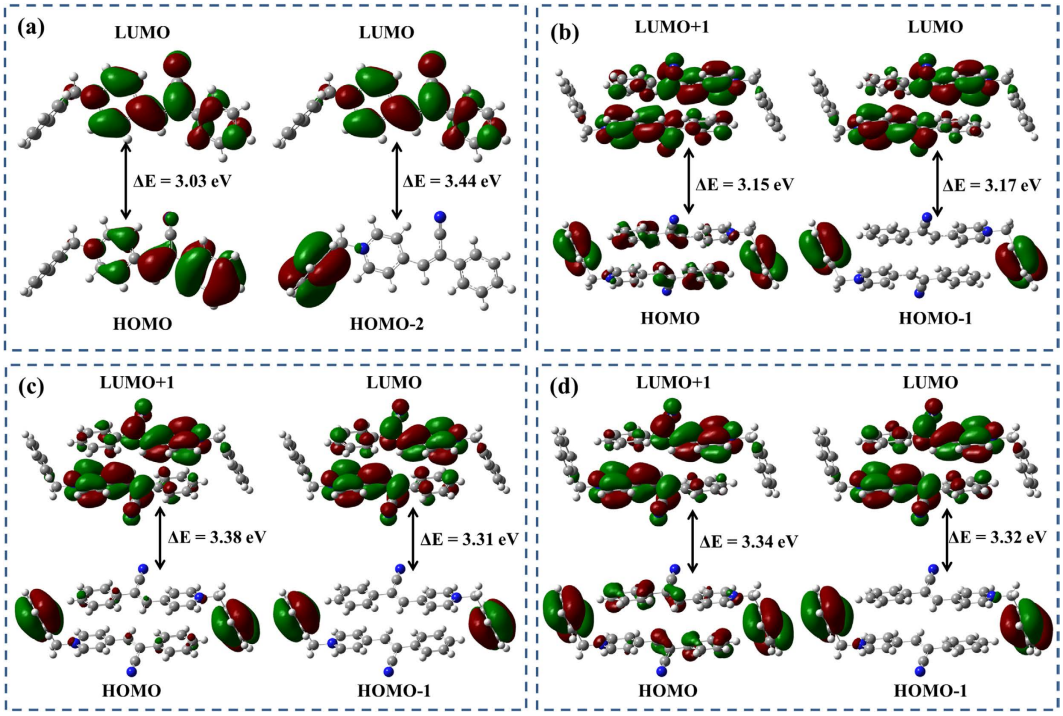

Figure 5. Selected frontier orbitals of the cationic monomer (**a**) and dimers of **PyCl** (**b**), **PyNO$_3$** (**c**) and **PyOTs** (**d**) at the singlet states.

PyCl (Figures S14–15). In **PyOTs**, the p-toluenesulfonate anions had H-bond interaction between two neighboring dimers. However, the steric effect of p-toluenesulfonate anions was dominated here, which was inserted in the space between dimers leading to the larger separation of 6.91 Å between dimers (Figure S16). The packing arrangements of cations in **PyPh$_4$B**, interestingly, are totally different to the other analogues. The large steric hindrance of tetraphenylboron anion impedes the electrostatic interactions of two cation fluorogens (Figure S17). The cations are "diluted" by the tetraphenylboron anions and present as single monomers in the crystal. The dimers are not formed and the electrostatic interactions take place of the intra/interdimeric interactions.

The solid-state fluorescence is ascribed to the decay of the dimeric excimers. These unique AIEEgens are different from other common ones with the mechanism of restriction of intramolecular rotations or intramolecular planarization. Steric hindrance of anions and the interactions between the anions and cations have dominating roles in the intra/interdimeric packing arrangements. Tetraphenylboron anions impede the formation of dimeric aggregates and result in very weak fluorescence of **PyPh$_4$B** in the solid state ($\Phi_F < 0.01$). On the other hand, **PyCl**, **PyNO$_3$**, and **PyOTs** form dimeric aggregates possess AIEE properties with strong emission in the solid state. The chloridion with small steric makes the **PyCl** easily form dimers. Its small intradimeric distance increases the π-conjugate overlap of the monomers, which induces the excimers emission. However, the strong π-π stacking opens the non-radiation channels, which results in relatively weak emission in the solid state. With the increasing of the steric hindrance of the anions, the intradimeric distance is increased. The decreased intradimeric π-π stacking leads to enhanced fluorescence of **PyNO$_3$** and **PyOTs** with blue-shifted emissions.

Furthermore, the formation of dimers in the solid state was supported by the evidence of fluorescence lifetimes. The dilute solutions of **PyCl**, **PyNO$_3$**, **PyOTs**, and **PyPh$_4$B** in acetonitrile exhibit very short fluorescence lifetime of ~0.3 ns. However, their fluorescence lifetimes in the solid state are dramatically different and dependent on the species of anions (Fig. 2). The fluorescence lifetime values of **PyCl**, **PyNO$_3$**, and **PyOTs** were 2.71 ns, 1.85 ns, and 7.81 ns, respectively. By contrast, **PyPh$_4$B** without dimers showed the shortest fluorescence lifetime that is comparable to the value measured in acetonitrile solution. The different fluorescence lifetimes and quantum yields of **PyCl** and **PyNO$_3$** in the solid state indicated that the strong interdimeric interactions did not decrease the emission but it would decrease the stability of excited state of dimers.

The electronic processes of monomer and dimer were also investigated by theoretical calculations. Frontier orbitals energy was illustrated in Table S2. The absorption of the monomer is attributed to transition of HOMO to LUMO and HOMO-2 to LUMO. As shown in Fig. 5, The electronic clouds of HOMO and LUMO located on the cyano substituted styrene unit and have no obviously separation that attributed to the π-π* transition. The HOMO-2 cloud distributes on the phenyl groups. The separation of HOMO-2 and LUMO demonstrates a strong ICT of D-σ-A. In dimers, the benzyl is conjugated through the π bond, which extends the π-conjugation areas. The intradimeric distance of two paralleled molecules conducts the overlap degree of π-conjugation. The intermolecular π-conjugation of **PyCl** are obviously overlap but those of **PyNO$_3$** and **PyOTs** are inconspicuous. However, the the strong CT and the appropriate intradimeric distance induce the through-space conjugation and result in the formation of a new lower intradimeric CT state. Furthermore, the fluorescence wavelength of

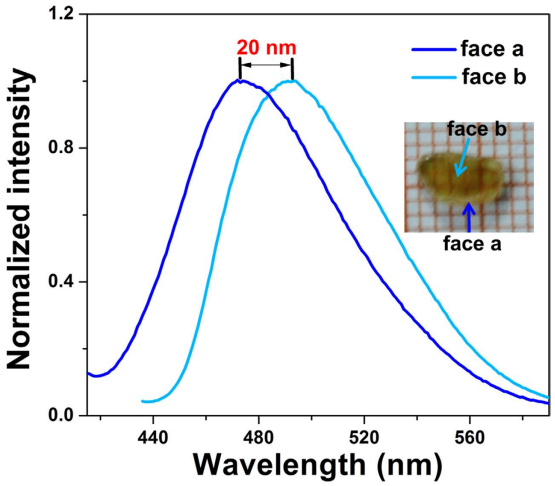

Figure 6. Fluorescence spectra of $PyNO_3$ crystal excited in different directions.

monomer and dimers of **PyCl**, **$PyNO_3$** and **PyOTs** were also calculated. The emission of monomer is at 416 nm. The emission wavelengths of dimers were red-shifted compared to monomer and the calculated wavelength of **PyCl**, **$PyNO_3$** and **PyOTs** dimers is 472, 437 and 439 nm, respectively. It shows that the dimers contain highly delocalized conjugated system. On the other hand, the calculated wavelength of **PyCl** and **PyOTs** dimer are approximate to the emission wavelength of solid state. But the calculated wavelength of **$PyNO_3$** is large blue shifted comparing to the experiments data. It indicated that the interdimeric distance also had effects on the solid emission. The **$PyNO_3$** interdimeric distance of is 3.58 Å smaller than that of **PyCl** and **PyOTs**. Thus, it demonstrates that both the interdimeric and intradimeric packing arrangements affect the fluorescence giving rise to the unique solid emission.

It is interesting that the special arrangement of dimers leads to anisotropic fluorescence of the crystals. It was fortunate that we obtained large volumetric crystals of **$PyNO_3$** ($5 \times 3 \times 1$ mm), which enable the measurement of anisotropic fluorescence convenient. As shown in Fig. 6, the crystal exhibit fluorescence peaks at 472 nm when it is excited perpendicular to face a. Excitation in the vertical direction of face b induces the emission of dimers, which was red-shifted of 20 nm. Owing to this interesting phenomenon, it may have great potential as anisotropic fluorescent probes for sensing applications.

Conclusions

In conclusion, we have demonstrated anion-controlled fluorescence of cyanostyryl-based pyridinium and investigated the mechanism at the molecular level. As the key role of anions in molecular packing arrangements, the synergy effects of anions' steric hindrance and the interactions with cations controlled the monomer-monomer and dimer-dimer distances, which highly affected the solid-state fluorescence. The unique dimeric packing endows the crystal of **$PyNO_3$** showing plane anisotropic fluorescence. This anion-controlled approach opens new guideline for the design of highly emissive functional materials.

Materials and instruments. All reagents were commercially available and used without further purification. All solvents were purified by conventional methods before used. UV-Vis spectra were recorded on a UV-3600 spectrometer with quartz cuvettes of 1.0 cm path length. The fluorescence spectra were recorded with a Hitachi F-7000 Fluorescence spectrometer. Fluorescence lifetime measurements were carried out using an HORIBA FluoroMax-4P fluorescence spectrometer equipped with a time-correlated single-photon counting (TCSPC) card. Absolute fluorescence quantum yields of solid state were determined by a calibrated integrating sphere. FT-IR spectra were obtained in KBr discs on a Nicolet 380 FT-IR spectrometer in the region of 4000–400 cm^{-1}. ^1H NMR and ^{13}C NMR were recorded on a Bruker Avance 400 MHz NMR spectrometer using $CDCl_3$ or DMSO-d_6 as solvent. Both ^1H and ^{13}C NMR were used tetramethylsilane ($SiMe_4$) as internal standards. NMR data were reported as follows: chemical shifts (δ) in ppm, multiplicity (s = singlet, d = doublet, t = triplet, m = multiplet), coupling constants J (Hz), integration, and interpretation. Mass spectra were recorded on an Agilent 6410 LC-MS/MS system (USA) equipped with an electrospray ion source (ESI). Silica gel 60 (200–300 mesh) was used for column chromatography. The time-dependent density functional theory (TD-DFT) implemented at the b3lyp/6–31 g* level using the Gaussian 09 program[59–62]. To improve calculation accuracy, the calculations were performed based on the crystal structure.

Synthesis of 2-(4-phenyl)-3-(4-pyridinyl)acrylonitrile. A mixture of 4-pyridinecarboxaldehyde 1.07 g (10 mmol) and phenylacetonitrile 1.17 g (10 mmol) in water (50 mL) was stirred at room temperature. Then, 8 mL 5% aqueous solution of NaOH was added by dropwise into the flask over 1 h. The mixture was sequentially stirred for another 12 h. The precipitate was filtered and washed with water. 1.94 g white solid was obtained, yielded 94%. ^1H NMR (DMSO-d_6, 400 MHz, ppm) δ: 8.77 (d, $J = 5.6$ Hz, 2 H), 8.11 (s, 1 H), 7.82 (d, $J = 6.4$ Hz, 4 H), 7.50–7.58

(m, 3 H). ^{13}C NMR (DMSO-d_6, 100 MHz, ppm) δ: 114.70, 116.97, 122.62, 126.13, 129.27, 130.07, 132.93, 140.20, 140.74, 150.43. HR-MS (ESI-MS): m/z = 207.0918, calcd for $(C_{14}H_{11}N_2)^+ = 207.0922$ ($[M+H]^+$).

Synthesis of compound PyCl. 2-(4-phenyl)-3-(4-pyridinyl)acrylonitrile (0.206 g, 1 mmol) was added to 5 mL benzyl chloride. The reaction was heated to reflux for overnight. After cooling down to room temperature, the mixture was filtered and the solid was washed with THF and toluene. The solid was dried under reduced pressure to give yellow wish solid 0.281 g, yielded 94%. FT-IR (KBr, cm^{-1}): 3423 (w), 3124 (w), 3027(s), 2968 (m), 2222 (w), 1637 (vs), 1603 (s), 1593 (m), 1556 (m), 1522 (m), 1496 (m), 1469 (m), 1454 (m), 1367 (w), 1350 (w), 1280 (w), 1261 (w), 1218 (w), 1208 (w), 1156 (s), 1077 (w), 1033 (w), 1003 (w), 932 (w), 920 (w), 853 (w), 815 (m), 767 (s), 742 (s), 705 (m), 686 (m), 671 (m), 611 (m), 550 (w), 523 (m), 452 (w). ^{1}H NMR (DMSO-d_6, 400 MHz, ppm) δ: 5.92 (s, 2 H), 7.47 (d, 3 H), 7.60 (t, 5 H), 7.89 (t, 2 H), 8.39 (s, 1 H), 8.51 (d, 2 H), 9.36 (d, 2 H). ^{13}C NMR (DMSO-d_6, 100 MHz, ppm) δ: 63.00, 116.15, 119.61, 126.74, 127.10, 128.97, 129.24, 129.43, 129.51, 131.31, 132.18, 134.20, 136.40, 145.22. HR-MS (ESI-MS): m/z = 297.1477, calcd for $(C_{21}H_{17}N_2)^+ = 297.1392$ ($[M\text{-}Cl]^+$).

Synthesis of compound $PyNO_3$. **PyCl** (0.166 g, 0.5 mmol) was dissolved in 5 mL MeOH and equimolar $AgNO_3$ was added. The mixture was vigorously stirred at room temperature for 3 h. then, the precipitate was filtered. The MeOH was evaporated under vacuum. Giving **$PyNO_3$** 0.167 g, yielded 93%.

Synthesis of silver p-toluenesulfonate. To 30 mL Na_2CO_3 (5.3 g, 0.05 mol) aqueous solution, 30 mL $AgNO_3$ (17 g, 0.1 mol) aqueous solution was added. The precipitate of Ag_2CO_3 was collected by filtration and washed with water. Then, Ag_2CO_3 was added to 200 mL water. To the suspension of Ag_2CO_3, p-toluenesulfonic acid monohydrate (19 g, 0.1 mol) was added. After stirring for 30 mins, a clear solution was obtained by filtration. The water was evaporated slowly on a hotplate to give 25.9 g white solid, yielded 93%.

Synthesis of compound PyOTs. **PyOTs** was prepared in a similar method to **$PyNO_3$**.

Synthesis of compound $PyPh_4B$. **PyCl** (0.66 g, 2.0 mmol) was dissolved in 10 mL MeOH, and then, 0.85 g tetraphenylborate in 10 mL EtOH was added. The mixture was stirred at room temperature for 10 mins. The precipitate was filtered and washed with water and MeOH to give **$PyPh_4B$** 0.92 g, yielded 74%.

References

1. Sun, D., Ren, Z., Bryce, M. R. & Yan, S. Arylsilanes and siloxanes as optoelectronic materials for organic light-emitting diodes (OLEDs). *J. Mater. Chem. C* **3,** 9496–9508 (2015).
2. Suzuri, Y., Oshiyama, T., Ito, H., Hiyama, K. & Kita, H. Phosphorescent cyclometalated complexes for efficient blue organic light-emitting diodes. *Sci. Technol. Adv. Mater.* **15,** 054202 (2014).
3. Uoyama, H., Goushi, K., Shizu, K., Nomura, H. & Adachi, C. Highly efficient organic light-emitting diodes from delayed fluorescence. *Nature* **492,** 234–238 (2012).
4. Visbal, R. & Gimeno, M. C. N-Heterocyclic carbene metal complexes: photoluminescence and applications. *Chem. Soc. Rev.* **43,** 3551–3574 (2014).
5. Zhang, T. *et al.* Efficient triplet application in exciplex delayed-fluorescence OLEDs using a reverse intersystem crossing mechanism based on a DeltaES-T of around zero. *ACS Appl. Mater. Interfaces* **6,** 11907–11914 (2014).
6. Chen, J. F., Gong, D. P., Wen, J., Ma, H. & Cao, D. K. 2-(Anthracenyl)-4,5-bis(2,5-dimethyl(3-thienyl))-1H-imidazole: regulatable stacking structures, reversible grinding- and heating-induced emission switching, and solid-state photodimerization behavior. *Chem. Sci.* **7,** 451–456 (2016).
7. Galer, P., Korosec, R. C., Vidmar, M. & Sket, B. Crystal structures and emission properties of the BF_2 complex 1-phenyl-3-(3,5-dimethoxyphenyl)-propane-1,3-dione: multiple chromisms, aggregation- or crystallization-induced emission, and the self-assembly effect. *J. Am. Chem. Soc.* **136,** 7383–7394 (2014).
8. Hu, T. *et al.* Effect of ionic interaction on the mechanochromic properties of pyridinium modified tetraphenylethene. *Chem. Commun.* **51,** 8849–8852 (2015).
9. Ma, Z. *et al.* A mechanochromic single crystal: turning two color changes into tricolored switch. *Angew. Chem. Int. Ed.* **55,** 519–522 (2016).
10. Park, S. K. *et al.* Stimuli-responsive reversible fluorescence switching in a crystalline donor-acceptor mixture film: mixed stack charge-transfer emission versus segregated stack monomer emission. *Angew. Chem. Int. Ed.* **55,** 203–207 (2016).
11. Ashton, T. D., Jolliffe, K. A. & Pfeffer, F. M. Luminescent probes for the bioimaging of small anionic species *in vitro* and *in vivo*. *Chem. Soc. Rev.* **44,** 4547–4595 (2015).
12. Kim, H. M. & Cho, B. R. Small-molecule two-photon probes for bioimaging applications. *Chem. Rev.* **115,** 5014–5055 (2015).
13. Li, Y. *et al.* Ultrasensitive near-infrared fluorescence-enhanced probe for *in vivo* nitroreductase imaging. *J. Am. Chem. Soc.* **137,** 6407–6416 (2015).
14. Sun, X., Wang, Y. & Lei, Y. Fluorescence based explosive detection: from mechanisms to sensory materials. *Chem. Soc. Rev.* **44,** 8019–8061 (2015).
15. Yang, Y., Zhao, Q., Feng, W. & Li, F. Luminescent chemodosimeters for bioimaging. *Chem. Rev.* **113,** 192–270 (2013).
16. Arjona-Esteban, A. *et al.* Influence of solid-state packing of dipolar merocyanine dyes on transistor and solar cell performances. *J. Am. Chem. Soc.* **137,** 13524–13534 (2015).
17. Beppu, T., Tomiguchi, K., Masuhara, A., Pu, Y. J. & Katagiri, H. Single benzene green fluorophore: solid-state emissive, water-soluble, and solvent- and pH-independent fluorescence with large stokes shifts. *Angew. Chem. Int. Ed.* **54,** 7332–7335 (2015).
18. Chaolumen, Murata, M., Sugano, Y., Wakamiya, A. & Murata, Y. Electron-deficient tetrabenzo-fused pyracylene and conversions into curved and planar π-systems having distinct emission behaviors. *Angew. Chem. Int. Ed.* **54,** 9308–9312 (2015).
19. Dou, J. H. *et al.* Fine-tuning of crystal packing and charge transport properties of BDOPV derivatives through fluorine substitution. *J. Am. Chem. Soc.* **137,** 15947–15956 (2015).
20. Jiménez, Á. J. *et al.* Structure-property relationships for 1,7-diphenoxy-perylene bisimides in solution and in the solid state. *Chem. Sci.* **5,** 608–619 (2014).
21. Moon, H. *et al.* Molecular-shape-dependent luminescent behavior of dye aggregates: bent versus linear benzocoumarins. *Cryst. Growth Des.* **14,** 6613–6619 (2014).
22. Wurthner, F. *et al.* Perylene bisimide dye assemblies as archetype functional supramolecular materials. *Chem. Rev.* **116,** 962–1052 (2016).
23. Zhu, Q. H. *et al.* Insight into the strong aggregation-induced emission of low-conjugated racemic C6-unsubstituted tetrahydropyrimidines through crystal-structure-property relationship of polymorphs. *Chem. Sci.* **6,** 4690–4697 (2015).

24. Bu, F. *et al.* Unusual aggregation-induced emission of a coumarin derivative as a result of the restriction of an intramolecular twisting motion. *Angew. Chem. Int. Ed.* **54,** 14492–14497 (2015).
25. Lu, H. *et al.* Highly efficient far red/near-infrared solid fluorophores: aggregation-induced emission, intramolecular charge transfer, twisted molecular conformation, and bioimaging applications. *Angew. Chem. Int. Ed.* **55,** 155–159 (2016).
26. Pan, C., Sugiyasu, K., Wakayama, Y., Sato, A. & Takeuchi, M. Thermoplastic fluorescent conjugated polymers: benefits of preventing π-π stacking. *Angew. Chem. Int. Ed.* **52,** 10775–10779 (2013).
27. Tang, X. *et al.* Efficient deep blue electroluminescence with an external quantum efficiency of 6.8% and CIEy < 0.08 based on a phenanthroimidazole-sulfone hybrid donor-acceptor molecule. *Chem. Mater.* **27,** 7050–7057 (2015).
28. Yang, J. X. *et al.* A facile synthesis and properties of multicarbazole molecules containing multiple vinylene bridges. *J. Am. Chem. Soc.* **127,** 3278–3279 (2005).
29. An, B. K., Kwon, S. K., Jung, S. D. & Park, S. Y. Enhanced emission and its switching in fluorescent organic nanoparticles. *J. Am. Chem. Soc.* **124,** 14410–14415 (2002).
30. Mei, J. *et al.* Aggregation-induced emission: the whole is more brilliant than the parts. *Adv. Mater.* **26,** 5429–5479 (2014).
31. Mei, J., Leung, N. L., Kwok, R. T., Lam, J. W. & Tang, B. Z. Aggregation-induced emission: together we shine, united we soar! *Chem. Rev.* **115,** 11718–11940 (2015).
32. Zhu, L. L. & Zhao, Y. L. Cyanostilbene-based intelligent organic optoelectronic materials. *J. Mater. Chem. C* **1,** 1059–1065 (2013).
33. He, X. *et al.* Polymorph crystal packing effects on charge transfer emission in the solid state. *Chem. Sci.* **6,** 3525–3532 (2015).
34. Liu, G., Liu, J., Liu, Y. & Tao, X. Oriented single-crystal-to-single-crystal phase transition with dramatic changes in the dimensions of crystals. *J. Am. Chem. Soc.* **136,** 590–593 (2014).
35. Zhu, W. *et al.* Revealing the charge-transfer interactions in self-assembled organic cocrystals: two-dimensional photonic applications. *Angew. Chem. Int. Ed.* **54,** 6785–6789 (2015).
36. Boydston, A. J. *et al.* Modular fluorescent benzobis(imidazolium) salts: syntheses, photophysical analyses, and applications. *J. Am. Chem. Soc.* **130,** 3143–3156 (2008).
37. Del Sesto, R. E. *et al.* Structure and magnetic behavior of transition metal based ionic liquids. *Chem. Commun.* 447–449 (2008).
38. Donald, W. A., Leib, R. D., Demireva, M. & Williams, E. R. Ions in size-selected aqueous nanodrops: sequential water molecule binding energies and effects of water on ion fluorescence. *J. Am. Chem. Soc.* **133,** 18940–18949 (2011).
39. Dong, M., Babalhavaeji, A., Hansen, M. J., Kalman, L. & Woolley, G. A. Red, far-red, and near infrared photoswitches based on azonium ions. *Chem. Commun.* **51,** 12981–12984 (2015).
40. Faul, C. F. Ionic self-assembly for functional hierarchical nanostructured materials. *Acc. Chem. Res.* **47,** 3428–3438 (2014).
41. Huang, Y. J., Jiang, Y. B., Bull, S. D., Fossey, J. S. & James, T. D. Diols and anions can control the formation of an exciplex between a pyridinium boronic acid with an aryl group connected via a propylene linker. *Chem. Commun.* **46,** 8180–8182 (2010).
42. Leontiev, A. V., Serpell, C. J., White, N. G. & Beer, P. D. Cation-induced molecular motion of spring-like [2]catenanes. *Chem. Sci.* **2,** 922 (2011).
43. Wang, Z. P. *et al.* $[Bmim]_2SbCl_5$: a main group metal-containing ionic liquid exhibiting tunable photoluminescence and white-light emission. *Chem. Commun.* **51,** 3094–3097 (2015).
44. Bell, N. A. *et al.* Comparison of the structure property relationships in LB films of zwitterionic TCNQ adducts. *J. Mater. Chem.* **15,** 1437 (2005).
45. Das, S. *et al.* Nontemplated approach to tuning the spectral properties of cyanine-based fluorescent nanoGUMBOS. *Langmuir* **26,** 12867–12876 (2010).
46. Hao, W. H., Yan, P., Li, G. & Wang, Z. Y. Short-conjugated zwitterionic cyanopyridinium chromophores: Synthesis, crystal structure, and linear/nonlinear optical properties. *Dyes and Pigments* **111,** 145–155 (2014).
47. Hinoue, T. *et al.* Regulation of π-stacked anthracene arrangement for fluorescence modulation of organic solid from monomer to excited oligomer emission. *Chem. Eur. J.* **18,** 4634–4643 (2012).
48. Mizobe, Y. *et al.* Systematic investigation of molecular arrangements and solid-state fluorescence properties on salts of anthracene-2,6-disulfonic acid with aliphatic primary amines. *Chem. Eur. J.* **15,** 8175–8184 (2009).
49. Sugino, M. *et al.* Elucidation of anthracene arrangement for excimer emission at ambient conditions. *Cryst. Growth Des.* **13,** 4986–4992 (2013).
50. Tohnai, N. *et al.* A facile and versatile approach to efficient enhancement of solid-state luminescence by organic-inorganic hybrid salts. *Dalton Trans.* **42,** 15922–15926 (2013).
51. Yao, H., Yamashita, M. & Kimura, K. Organic styryl dye nanoparticles: synthesis and unique spectroscopic properties. *Langmuir* **25,** 1131–1137 (2009).
52. Bhattacharya, S. & Samanta, S. K. Unusual salt-induced color modulation through aggregation-induced emission switching of a bis-cationic phenylenedivinylene-based π hydrogelator. *Chem. Eur. J.* **18,** 16632–16641 (2012).
53. Zhao, N. *et al.* Effect of the counterion on light emission: a displacement strategy to change the emission behaviour from aggregation-caused quenching to aggregation-induced emission and to construct sensitive fluorescent sensors for Hg^{2+} detection. *Chem. Eur. J.* **20,** 133–138 (2014).
54. Yao, L. *et al.* Highly efficient near-infrared organic light-emitting diode based on a butterfly-shaped donor-acceptor chromophore with strong solid-state fluorescence and a large proportion of radiative excitons. *Angew. Chem. Int. Ed.* **53,** 2119–2123 (2014).
55. Chen, C. *et al.* Photo-facilitated aggregation and correlated color temperature adjustment of single component organic solid state white-light emitting materials. *J. Mater. Chem. C* **3,** 4563–4569 (2015).
56. Kim, M., Whang, D. R., Gierschner, J. & Park, S. Y. A distyrylbenzene based highly efficient deep red/near-infrared emitting organic solid. *J. Mater. Chem. C* **3,** 231–234 (2015).
57. Mallia, A. R., Salini, P. S. & Hariharan, M. Nonparallel stacks of donor and acceptor chromophores evade geminate charge recombination. *J. Am. Chem. Soc.* **137,** 15604–15607 (2015).
58. Wang, L. *et al.* Red emissive diarylboron diketonate crystals: aggregation-induced color change and amplified spontaneous emission. *J. Mater. Chem. C* **3,** 499–505 (2015).
59. Frisch, M. J. *et al.* Gaussian 09, Revision E.01. Gaussian, Inc., Wallingford CT, USA. URL http://www.gaussian.com/ (2009).
60. Becke, A. D. Density-functional thermochemistry. III. The role of exact exchange. *J. Chern. Phys.* **98,** 5648–5652 (1993).
61. Lee, C., Yang, W. t. & Parr, R. G. Development of the Colle-Salvetti correlation-energy formula into a functional of the electron density. *Phys. Rev. B* **37,** 785–789 (1988).
62. Miehlich, B., Savin, A., Stoll, H. & Preuss, H. Results obtained with the correlation energy density functionals of becke and Lee, Yang and Parr. *Chem. Phys. Lett.* **157,** 200–206 (1989).

Acknowledgements

This work was supported by Educational Commission of Anhui Province of China (KJ2014ZD02), the National Natural Science Foundation of China (51432001), Macao Science and Technology development Fund under grant No.: 052-2015-A2 and Start-up research grant of University of Macau (SRG2015-00007-FHS).

Author Contributions

G.B. contributed to the design of the experiments and wrote the manuscript. X.J. and J.X. supervised the whole project and revised the manuscript. L. improved the experiment plan and analyzed X-ray single crystal structures. S.C. synthesized the intermediate of compounds. Y.P. and X.T. contributed to the analysis and discussion on the experimental data and also revised the manuscript. All authors reviewed the manuscript.

Additional Information

Supplementary information accompanies this paper at http://www.nature.com/srep

Competing financial interests: The authors declare no competing financial interests.

How to cite this article: Zhang, G. *et al.* Anion-controlled dimer distance induced unique solid-state fluorescence of cyano substituted styrene pyridinium. *Sci. Rep.* **6**, 37609; doi: 10.1038/srep37609 (2016).

Publisher's note: Springer Nature remains neutral with regard to jurisdictional claims in published maps and institutional affiliations.